

Video Face Clustering with Unknown Number of Clusters

Makarand Tapaswi^{1,2,3} Marc T. Law^{2,3,4} Sanja Fidler^{2,3,4}

¹Inria ²University of Toronto ³Vector Institute ⁴NVIDIA

makarand.tapaswi@inria.fr, {makarand, law, fidler}@cs.toronto.edu

https://github.com/makarandtapaswi/BallClustering_ICCV2019

Abstract

Understanding videos such as TV series and movies requires analyzing who the characters are and what they are doing. We address the challenging problem of clustering face tracks based on their identity. Different from previous work in this area, we choose to operate in a realistic and difficult setting where: (i) the number of characters is not known a priori; and (ii) face tracks belonging to minor or background characters are not discarded.

To this end, we propose Ball Cluster Learning (BCL), a supervised approach to carve the embedding space into balls of equal size, one for each cluster. The learned ball radius is easily translated to a stopping criterion for iterative merging algorithms. This gives BCL the ability to estimate the number of clusters as well as their assignment, achieving promising results on commonly used datasets. We also present a thorough discussion of how existing metric learning literature can be adapted for this task.

1. Introduction

Characters are a central aspect of any story. While video streaming platforms such as Netflix provide the ability to find a movie based on metadata, searching a video collection to find the right clip when “Jack Sparrow first meets Will” requires analyzing the content of the video. Understanding characters also has a direct influence on important research problems such as video captioning [34, 35], question-answering [22, 44], and studying social situations [45].

Characters are often studied by analyzing face tracks (sequences of temporally related detections) in videos. A significant part of this analysis is *identification* - labeling face tracks with their names, and typically employs supervision from web images [1, 29], transcripts [3, 9], or even dialogs [7, 15]. We are interested in an equally popular alternative - *clustering* face tracks based on identity. Note that clustering is complementary to identification, and if achieved successfully can dramatically reduce the amount of required labeling effort. Clustering is also an interesting problem in itself as it can answer questions such as who are the main characters, or what are their social interaction groups.



Figure 1. Video face clustering is a challenging problem that is further accentuated by a large portion of characters that play small roles. Can you guess how many characters are in this montage and which faces belong to them? See Fig. 2 for our solution.

While there exists a large body of work in video face clustering (e.g. [6, 18, 55]), most of it addresses a simplified setup where background characters¹ are ignored and the total number of characters is known. With recent advances in face representations [4], their application towards clustering [38], and the ability to learn cast-specific metrics by looking at overlapping face tracks [6], we encourage the community to address the challenging problem of estimating the number of characters and not ignoring background cast (see Fig. 1).

In this paper, we propose *Ball Cluster Learning* (BCL) - a supervised approach to carve the embedding space into equal-sized balls such that samples within a ball belong to one cluster. In particular, we formulate learning constraints that create such a space and show how the ball radius (also learned) can be associated with the stopping criterion for agglomerative clustering to estimate both the number of clusters and assignment (Sec. 3). We demonstrate BCL on video face clustering in a setup where we are unaware of the number of characters, and *all* face tracks, main character or otherwise, are included (Sec. 4). Thus, BCL is truly applicable to all videos as it does not place assumptions on availability of cast lists (to determine number of clusters) or track labels (to discard background characters). To evaluate our approach, we augment standard datasets used in video

¹We consider three types of characters based on their roles: *primary* or *recurring* characters have major roles in several episodes; *secondary* or *minor* characters are named and play an important role in some episodes; and *background* or *unknown* (Unk) characters are unnamed and uncredited.

face clustering by resolving labels between all background characters. Our approach achieves promising results in estimating the number of clusters and the cluster assignment. We also present a thorough analysis of commonly used loss functions in verification (*e.g.* contrastive loss), compare them against BCL, and discuss how and when they may be suitable for clustering. To the best of our knowledge, BCL is the first approach that learns a threshold to estimate the number of clusters at test time. Code and data are available at Github.

2. Related Work

We survey work on identifying and clustering characters in videos. We also review metric learning approaches, some of which are adopted for clustering in this work (Sec. 3.4).

Character identification in videos. Over a decade earlier, the availability of transcripts (speaker names and dialogs) and their alignment with subtitles (dialogs and timestamps) opened exciting avenues for fully automatic identification [3, 9, 33, 40]. Dialog-based supervision proved to be a harder but scalable approach [7, 15]. Face track representations (*e.g.* [23, 30, 31, 48, 53]) further improved performance. Recently, the source of supervision moved towards web images from IMDB [1, 45] or image search [29], and a combination of modalities such as hair [29], speech [28] and clothing [42]. However, these advances are limited to identifying named characters and grouping all remaining characters in a common “others” label.

Video face clustering. A common idea adopted by many clustering approaches is to use unsupervised constraints that arise from the video to learn cast-specific metrics [6]. Pairs of face images within tracks are considered similar; and faces that appear simultaneously in the video are assumed dissimilar. These constraints are used with Hidden Markov Random Fields [49, 50], or to learn low-rank block-sparse representations [51]. They also see use in conjunction with the video editing structure (shots, threads, and scenes) [43]. The constraints are also used to fine-tune CNNs and learn clustering jointly [55], or to learn an embedding using an improved triplet loss [54].

Recently, an end-to-end detection and clustering approach considers false positive and missed detections [18]. Ignoring tracks, metrics are learned by ranking a batch of frames and creating hard positive and negative pairs [39]. However, all of the above methods require knowledge of the number of clusters K that is difficult to estimate beforehand; and only consider primary characters (tracks for background characters are ignored). In online face clustering spatiotemporal constraints along with CNN representations are used to assign a new track to existing or new cluster [19]. However, only primary characters in the video are targeted.

In this paper, we consider a setup where *all* face tracks are to be clustered into an *unknown* number of characters.

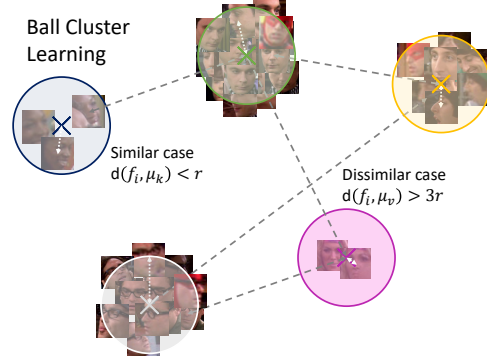


Figure 2. The face tracks in Fig. 1 can be clustered into 5 characters. *Ball Cluster Learning* carves the feature space into balls of equal radius. The number of samples in the cluster does not affect the ball radius or minimum separation to other balls.

Metric learning. Early examples of state-of-the-art approaches in face recognition adopt metric learning [5, 12]. The learning task is often posed as verification - are two face images of the same person. The main difficulty is ensuring that the model generalizes to test images of people that are not seen during training. When working with videos, this is mitigated by obtaining positive and negative pairs through tracking and training on the video itself.

Other loss functions involving *triplets* [37] are also proposed for face verification [36]. While FaceNet [36] claims to be good at clustering, performance is only evaluated qualitatively. Training with the triplet loss is cumbersome as it requires creation of all possible triplets that is computationally expensive. Sampling strategies become crucial to ensure fast convergence while avoiding degenerate solutions.

Centroid-based losses [20, 21, 26, 41] are also proposed for face verification [46]. Here, models are trained to make each sample closer to the representative of its category than to the representative of any other category resulting in samples of the same category being grouped into a single cluster. These methods are ideal when the number of clusters is known at test time. However, there is neither a constraint on the size/radius of the clusters, nor is there a threshold to predict whether two samples are similar, *e.g.* NormFace [46] trains a classifier to determine whether pairs are similar.

Joint Unsupervised LEarning (JULE) [52] learns representations while performing hierarchical clustering. However, as JULE has to learn both the cluster assignments and representations, it is hard to scale [10, 11, 27] and its computational cost and memory complexity are extremely high. Moreover, JULE is only tested in cases where the number of clusters is known at test time.

We propose a model that groups similar samples into non-overlapping balls. The radius of the ball clusters is learned and is directly related to the threshold used as a stopping criterion of our clustering algorithm (Sec. 3.3). In addition, our training algorithm has very low algorithmic complexity: it is linear in the batch size and in the number of clusters.

3. Ball Cluster Learning (BCL)

The main goal of our supervised learning approach is to carve the embedding space into balls with a shared but trainable radius for each cluster, while simultaneously creating a well-defined separation between balls of different cluster labels (Fig. 2). We first define the constraints that achieve the above goal (Sec. 3.1), formulate the learning problem with loss functions (Sec. 3.2), and then explain how to perform clustering at test time (Sec. 3.3). Finally, we review several losses from the metric learning literature that may be suitable for clustering (Sec. 3.4).

Notation. Let $B = \{(x_i, y_i)\}_{i=1}^N, y_i \in \{1, \dots, K\}$ be a mini-batch containing N samples that we wish to group into K clusters. We learn a mapping $\varphi_\theta : \mathcal{X} \rightarrow \mathcal{F}$ (e.g. a neural network) parameterized by θ . The embedding space can either be $\mathcal{F} = \mathbb{R}^D$ or $\mathcal{F} = \mathbb{S}^{D-1} = \{\mathbf{f} \in \mathbb{R}^D : \|\mathbf{f}\|_2 = 1\}$ inspired by recent work [46] that shows benefits of ℓ_2 normalization for face recognition. The i -th sample is represented by the output of the mapping $\mathbf{f}_i = \varphi_\theta(x_i)$.

“Ball” terminology: We define samples of our clusters as lying in a ball. However, when $\mathcal{F} = \mathbb{S}^{D-1}$, our clusters technically lie on the hypersurface of *hyperspherical cones*.

3.1. Constraints

We analyze similar and dissimilar samples separately. Let \mathcal{C}_k be the k -th set of similar samples (i.e. samples x_i that satisfy $y_i = k$). A pair of samples (x_i, x_j) is similar iff $y_i = y_j$, and it is dissimilar otherwise.

Similar case. We define $\mu_k \in \mathcal{F}$ as the centroid of all the samples in \mathcal{C}_k w.r.t. the squared Euclidean distance:

$$\mu_k = \frac{1}{\nu_{\mathcal{F}}} \sum_{x_i \in \mathcal{C}_k} \mathbf{f}_i \in \arg \min_{\mu \in \mathcal{F}} \sum_{x_i \in \mathcal{C}_k} d^2(\mathbf{f}_i, \mu), \quad (1)$$

where $d : \mathcal{F} \times \mathcal{F} \rightarrow \mathbb{R}$ is the Euclidean distance (i.e. $d^2(\mathbf{f}_i, \mu_k) = \|\mathbf{f}_i - \mu_k\|_2^2$). The factor $\nu_{\mathcal{F}}$ is N if $\mathcal{F} = \mathbb{R}^D$, or $\|\sum_{x_i \in \mathcal{C}_k} \mathbf{f}_i\|_2$ (we assume for simplicity that it is non-zero) if $\mathcal{F} = \mathbb{S}^{D-1}$ since μ_k is constrained to be in \mathcal{F} (on the unit-norm hypersphere). For any sample x_i that belongs to \mathcal{C}_k , we would like to learn a representation \mathbf{f}_i such that its squared distance to μ_k is smaller than some learned threshold $b > 0$. Our goal is to satisfy the constraints:

$$\forall x_i \in \mathcal{C}_k, d^2(\mathbf{f}_i, \mu_k) \leq b. \quad (2)$$

Note that b is trained as a model parameter. We consider that the *radius* r of the balls is $r = \sqrt{b} \geq \max_{x_i \in \mathcal{C}_k} d(\mathbf{f}_i, \mu_k)$. By using the triangle inequality, similar samples satisfy the following constraint:

$$\forall x_i \in \mathcal{C}_k, x_j \in \mathcal{C}_k, d(\mathbf{f}_i, \mathbf{f}_j) \leq 2r = 2\sqrt{b}. \quad (3)$$

We choose $2r$ as the threshold to determine whether two samples are similar or not.

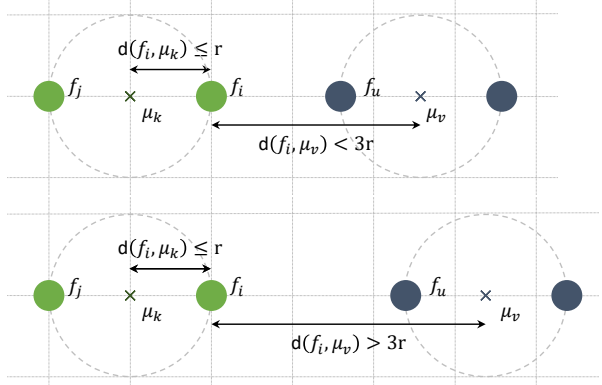


Figure 3. Consider a toy scenario with 4 samples (2 green, 2 blue in each cluster) in $\mathcal{F} = \mathbb{R}^2$. We illustrate the constraints derived in Eq. (2) and Eq. (4). Each grid square in this 2D-space corresponds to the ball radius r . **Top:** When $d(\mathbf{f}_i, \mu_v) < 3r$, we see that \mathbf{f}_i and \mathbf{f}_u are the closest samples and will be merged by hierarchical agglomerative clustering (HAC) in the first iteration. **Bottom:** When $d(\mathbf{f}_i, \mu_v) > 3r$, the distance between \mathbf{f}_i and \mathbf{f}_u is larger than either the green or blue pair of samples. Additionally, by adopting the max linkage and choosing the stopping criterion for HAC as $\tau = 2r$ (in Euclidean distance), iterative merging stops after the green and blue samples are grouped. Best seen in color.

Dissimilar case. From the above discussion, two dissimilar samples (x_i, x_u) should satisfy $d(\mathbf{f}_i, \mathbf{f}_u) > 2r$. Furthermore, as the distance between $x_u \in \mathcal{C}_v$ and its centroid μ_v is at most r , the Euclidean distance between \mathbf{f}_i and μ_v should be greater than $3r$ to ensure that all the clusters are separated (see Fig. 3). This implies $d^2(\mathbf{f}_i, \mu_v) > (3r)^2 = 9b$. We denote $\gamma = 9b + \varepsilon$ where $\varepsilon \geq 0$ is a small fixed margin and formulate the constraint:

$$\forall x_i \in \mathcal{C}_k \neq \mathcal{C}_v, d^2(\mathbf{f}_i, \mu_v) \geq \gamma. \quad (4)$$

A major difference to existing metric learning approaches is that we enforce an upper bound on the distance between each example and its desired centroid (Eq. (2)), which in turn enforces samples of each cluster to be within a ball of radius r . We also enforce different clusters to be separated by a margin that is a function of the radius (Eq. (4)).

Computational complexity. Formulating our constraints on the distances between samples and cluster centroids significantly lowers the number of computations in contrast to pairwise distances that yield quadratic constraints.

A fixed radius for all balls allows us to use it as a threshold to delimit clusters. In addition, it has the potential to address the long-tail since each identity gets the same volume of embedding-space, agnostic to the number of tracks.

3.2. Problem Formulation

Based on the desired constraints in Sec. 3.1, we now formulate an optimization problem that tries to satisfy them. Our goal is to learn the squared radius $b > 0$ of the cluster

balls and parameters θ of the model φ_θ that minimize the objective problem \mathcal{L}_{ball} defined as the sum of the two losses:

$$\mathcal{L}_{ball} = \alpha \mathcal{L}_{sim} + \mathcal{L}_{dis}, \quad (5)$$

where $\alpha \geq 0$ is a hyperparameter to balance the losses. We present details of the loss terms in the following.

The goal of the loss \mathcal{L}_{sim} is to satisfy the similar pairs constraint in Eq. (2), and is formulated as:

$$\mathcal{L}_{sim} = \frac{1}{N} \sum_{x_i \in \mathcal{C}_k} [d^2(\mathbf{f}_i, \boldsymbol{\mu}_k) - b]_+, \quad (6)$$

where $[x]_+ = \max(0, x)$. In the context of metric learning, this often corresponds to the *positive* loss as it brings together samples of the same cluster.

The goal of the dissimilar loss \mathcal{L}_{dis} is to satisfy dissimilar pairs constraints in Eq. (4) and is formulated as:

$$\mathcal{L}_{dis} = \frac{1}{N} \sum_{x_i \in \mathcal{C}_k} \max_{v \neq k} [\gamma - d^2(\mathbf{f}_i, \boldsymbol{\mu}_v)]_+. \quad (7)$$

This loss aims to push away from the *most* offending cluster centroid by employing $\max_{v \neq k}$, and is equivalent to hard negative mining in metric learning [36].

3.3. Clustering Algorithm

We now describe how to perform clustering and predict the number of clusters on some given (test) dataset. Recall that we are interested in solving problems where the number of clusters is unknown at test time.

As explained in Sec. 3.1, our constraints are formulated so that similar samples should satisfy $d^2(\mathbf{f}_i, \mathbf{f}_j) \leq 4b$ and dissimilar samples should have larger distances. We apply a clustering algorithm which groups pairs of examples that satisfy those constraints into a single cluster.

Even when the number of clusters is known, finding the partitions that minimize some clustering energy function is an NP-hard problem [2]. Thus, methods that find a good local minimum solution with reasonable complexity are often used (e.g. K -means [24]). For this reason, we adopt the Hierarchical Agglomerative Clustering (HAC) method [8]: each sample starts in its own cluster, and pairs of clusters are iteratively merged until some specific stopping criterion. In the context of *complete linkage*, two clusters U and V are merged into a single cluster if they minimize:

$$\ell_{complete}(U, V) = \max_{x_u \in U, x_v \in V} d^2(\mathbf{f}_u, \mathbf{f}_v). \quad (8)$$

Let us denote $\tau > 0$ the threshold chosen such that the HAC algorithm stops when there are *no* two clusters U and V that satisfy $\ell_{complete}(U, V) \leq \tau$. Once the HAC algorithm stops, all the examples assigned to a same cluster U satisfy $\forall x_a \in U, x_b \in U, d^2(\mathbf{f}_a, \mathbf{f}_b) \leq \tau$ by definition of the complete linkage. Thus, we choose $\tau = 4b$. With this value of

τ , when the (ideal) global minimum of Eq. (5) is obtained, applying the HAC with linkage in Eq. (8) groups similar examples in the same clusters and separates dissimilar examples since both Eq. (3) and Eq. (4) are satisfied.

3.4. Extending related work to our task

We compare BCL with various metric learning approaches commonly used in face verification tasks.

Triplet Loss [36] tries to preserve the order of distances between similar pairs (x_i, x_j) and dissimilar pairs (x_i, x_u) : $\mathcal{L}_{triplet} = \sum_{\substack{y_i=y_j \\ y_i \neq y_u}} [d^2(\mathbf{f}_i, \mathbf{f}_j) - d^2(\mathbf{f}_i, \mathbf{f}_u) + m]_+$. While the loss ensures that positives are closer than negatives by a margin m , there is no constraint on the distance between positive samples. Thus, we are unable to directly use the margin as a threshold for stopping the HAC algorithm.

Threshold strategy. We choose a threshold based on a validation set: we apply the HAC algorithm and pick the threshold that predicts the ground truth number of validation clusters. Even for the baselines that learn a threshold, this strategy worked better than using the learned threshold. Thus, we report scores using this strategy for all baselines.

Contrastive Loss [5] considers pairwise constraints. For any pair of samples (x_i, x_j) , and $y_{ij} = 1$ when they are similar and 0 otherwise, the contrastive loss between them is $\mathcal{L}_{cont} = \frac{y_{ij}}{2} d^2(\mathbf{f}_i, \mathbf{f}_j) + \frac{1}{2} (1 - y_{ij}) [m - d(\mathbf{f}_i, \mathbf{f}_j)]_+^2$. This aims to make dissimilar samples at least m distance apart. While m is usually a fixed hyperparameter, we treat it as a trainable value in the same way as b in BCL.

Logistic Discriminant Metric Learning (LDML) [12] maps distances to a probability score via the sigmoid function $\sigma(\cdot)$. It can be written as $p_{ij} = p(y_i = y_j | \mathbf{f}_i, \mathbf{f}_j, \beta) = \sigma(\beta - d^2(\mathbf{f}_i, \mathbf{f}_j))$, where β is a threshold trained to distinguish similar from dissimilar pairs. The loss is formulated as binary cross-entropy and is minimized: $\mathcal{L}_{ldml} = -\sum_{y_i=y_j} \log p_{ij} - \sum_{y_i \neq y_j} \log(1 - p_{ij})$.

Prototypical Networks [41] If both Eq. (2) and Eq. (4) are satisfied, the following order is obtained: $\forall x_i \in \mathcal{C}_k, v \neq k, d^2(\mathbf{f}_i, \boldsymbol{\mu}_k) - b \leq d^2(\mathbf{f}_i, \boldsymbol{\mu}_v) - \gamma$. To satisfy this relative constraint, we formulate the cross entropy loss:

$$\mathcal{L}_{proto} = -\frac{1}{N} \sum_{i \in \mathcal{C}_k} \frac{1}{|\mathcal{C}_k|} \log(p(y_i = k | \mathbf{f}_i)) \quad (9)$$

where $p(y_i = k | \mathbf{f}_i)$ is the posterior probability:

$$\frac{\exp(-d^2(\mathbf{f}_i, \boldsymbol{\mu}_k) + b)}{\exp(-d^2(\mathbf{f}_i, \boldsymbol{\mu}_k) + b) + \sum_{v \neq k} \exp(-d^2(\mathbf{f}_i, \boldsymbol{\mu}_v) + \gamma)}. \quad (10)$$

The vanilla Prototypical Networks [41] correspond to \mathcal{L}_{proto} when $b = \gamma = 0$. NormFace [46] is similar to [41], with one main difference that representations are ℓ_2 -normalized. We report scores for $b = \gamma = 0$ since we experimentally found that it returns the best results with our threshold strategy.

4. Video Face Track Clustering with BCL

We discuss how BCL can be applied to face track clustering. Each sample represents a face track and is associated with a specific identity. Our goal is to create clusters such that tracks with the same identity are grouped together.

During training, we create mini-batches by uniformly sampling a fixed number of tracks. As the training data contains several identities with very few (1-2) tracks, and many others with hundreds or thousands of tracks, uniform random sampling preserves the skewed distribution of cluster membership within the mini-batch (see Fig. 4). From each track, we randomly choose one face image (which serves as data augmentation) and use a pre-trained and fixed CNN to extract a face representation x_i . We will refer to this as the base CNN representation. At test time, we average the base representations of all face images in the track and apply HAC after computing embeddings. This makes the track feature robust, while keeping it in the same space as the training samples. Other track-level representations such as [23, 30, 48, 53] are out of scope of this work.

Base CNN is a 50-layer ResNet [16] with squeeze-and-excitation (SE) blocks [17]. The model is pre-trained on the MS-1M dataset [13], and fine-tuned on the VGGFace2 dataset [4] with cross-entropy loss to predict over 8000 identities. We obtain features in \mathbb{R}^{256} from the last layer (before the classifier). This model is named SE-ResNet50-256.² We will show that our methods work equally well when using a different base CNN. We do not fine-tune the CNN.

Model. Our model φ_θ is a stack of 4 linear layers with ReLU non-linearity (MLP) in between and is applied on top of the base CNN representation. When not stated otherwise, the hidden layers have 256, 128, and 64 nodes, and the final embedding dimension $D = 64$.

Our constraints require that $b > 0$. To this end, we use the `softplus` operator defined as $b = \log(1 + e^{\hat{b}})$, and train $\hat{b} \in \mathbb{R}$ as a model parameter. We balance the similar and dissimilar losses with $\alpha = 4$ based on the performance on a validation set.

Learning. We find that the loss for our model can be reduced dramatically (to ϵ) by mapping all samples to the same point and learning the squared radius to be close to 0. We prevent the learning process from reducing the radius to 0, by freezing it for the first 5 epochs. Subsequently, the loss parameter \hat{b} updates slowly, 0.1 times the learning rate used for MLP weights. We employ SGD with 0.9 momentum at a learning rate of 0.003, and a $0.9\times$ decay every 10 epochs to update the weights of the MLP. We use mini-batches of 2000 samples (tracks) when not stated otherwise.

²We use the pre-trained PyTorch model provided by https://github.com/ox-vgg/vgg_face2.

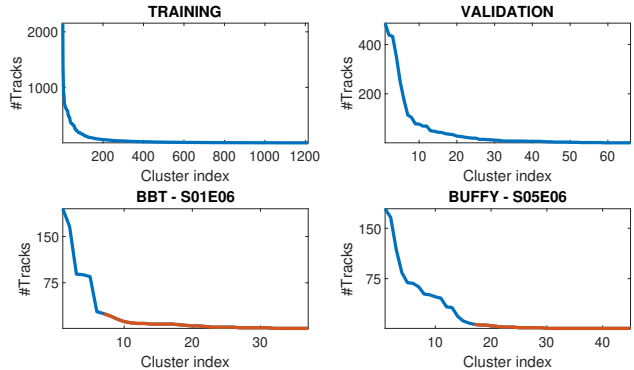


Figure 4. Number of tracks in clusters. Orange lines in BBT and BUFFY indicate track counts for unknown/background characters.

5. Evaluation

We first present the datasets and metrics used in our experiments. Then, we perform ablation studies on the validation split and finally show and discuss our results on the test set.

5.1. Datasets and metrics

We use face tracks from several movies and TV series as part of training and evaluation.

Train and validation splits consist of face tracks and ground-truth identity labels provided for 51 movies from the MovieGraphs dataset [45]. Like most previous work, the dataset contains annotations for main characters only, and does not disambiguate between background characters. Nevertheless, it is suitable for training, and we obtain 65,076 tracks that are mapped to 1,280 unique actors using IMDb. As Fig. 4 indicates, many actors have few (and even one) tracks making the training distribution similar to test.

We reserve 5% of the actors for validation and ensure that actors appearing in the test data are *not* seen during train or validation. This results in 61,774 tracks (1,214 actors) for the train split and 3,302 tracks (66 actors) for validation.

Test split. Our evaluation is on six episodes each of two TV series: The Big Bang Theory (BBT) and Buffy the Vampire Slayer (BUFFY). Both have been actively used in person identification and clustering [3, 18, 39, 55].³ We wish to emphasize that most previous approaches for face clustering only consider primary (recurring) characters and know the number of clusters. We adopt a more practical setting where the number of characters is *not* known, and tracks for *all* (secondary as well as background characters) are included. We painstakingly resolve faces of background characters and assign unique identifiers to them. This is difficult even for humans, but is achieved through a combination of facial (hair) and non-facial (clothing, spatial location) cues. Finally, we also evaluate on *combined tracks* from several episodes

³We use an updated version of the tracks that does not discard background characters and small/profile faces.

	One cluster	N clusters	Base K known	Ours $\tau = 4b$
#Cl	1	3302	66	69
NMI	0	0	68.91	77.09
WCP	14.75	100.0	76.53	85.65

Table 1. Performance on the validation set showing the impact of putting all samples in the same or their own clusters. We also present performance of base CNN features when the number of clusters is known. The validation set has 66 ground-truth clusters.

Base CNN	Dim	#P	#Cl	NMI	WCP
SE-ResNet50-256	256	26.5M	69	77.09	85.65
ResNet50	2048	41.1M	80	76.74	87.67

Table 2. Performance on validation set for different base CNN models. The 4-layer MLP used for the ResNet50 model is $2048 \rightarrow 512 \rightarrow 256 \rightarrow 128 \rightarrow 64$.

Dim	256	128	64	32	16	8
#P	263K	132K	111K	109K	108K	107K
#Cl	45	62	69	68	72	29
NMI	76.68	76.89	77.09	75.48	68.72	47.62
WCP	81.98	85.52	85.65	85.89	79.35	50.79

Table 3. Performance on the validation set for varying embedding dimension. #P indicates the number of parameters in the MLPs.

(and series) to mimic additional challenging scenarios. Each face in Fig. 1 represents a different track from BBT-S1E1.

Metrics. We adopt three primary metrics to evaluate performance: (i) #Cl: is the number of predicted clusters, and should be close to the ground-truth number of identities. (ii) Normalized Mutual Information (NMI) [25]: for a given set of class labels Y and cluster predictions C , NMI is calculated as $2I(Y; C)/(H(Y) + H(C))$, where $H(\cdot)$ is entropy, and $I(\cdot; \cdot)$ is mutual information. NMI is a balanced metric and scores 0 when all samples are either in one cluster or their own clusters (see Table 1). All model checkpoints are chosen to maximize NMI on the validation set. (iii) Weighted Clustering Purity (WCP) [43]: Also called clustering accuracy [55], WCP combines purity (fraction of samples that belong to the same class) of the clustering by weighting with the number of samples in the cluster.

5.2. Ablation Studies

We make several design choices that are motivated in the following. Table 1 provides insights into the validation split by showing the extreme ends of the clustering. We also demonstrate that our model outperforms the base CNN descriptors even when the base model is assumed to know the actual number of clusters (Base K known). Throughout this section, the ideal number of clusters on validation is 66.

Base CNN model. We demonstrate that the choice of the CNN model does not directly influence performance. In fact, our base model SE-ResNet50-256 has an output space $x_i \in$

	Batch size	500	1000	2000	4000
#Cl	in batch	220	330	450	600
(approx)	> 5 samples	15	45	90	150
Performance	#Cl	88	91	69	29
on	NMI	72.13	74.63	77.09	76.55
Validation	WCP	83.77	87.28	85.65	79.68

Table 4. Ablation studies on mini-batch size. The first half of the table reports the number of the clusters in the batch, and those that have more than 5 samples. In the second half, we report performance on validation.

\mathbb{R}^{256} while the ResNet50 base model produces $x_i \in \mathbb{R}^{2048}$. Table 2 shows that both models exhibit similar performance.

Embedding dimension. From the results in Table 3, we can infer that choosing too small an embedding dimension reduces performance dramatically. However, setting $D \geq 32$ achieves comparable similar performance.

Batch size. Our model learns to satisfy the constraints and perform clustering on data within each mini-batch. When batches are small (*e.g.* less than 50) it is likely that most clusters have only one sample. This automatically satisfies positive constraints and gradients are 0. Making the mini-batches too large incurs a computational cost and reduces the number of parameter updates; the model requires many more epochs to reach a similar performance. In Table 4, we first report the approximate number of clusters in a batch, and the number of clusters with more than 5 samples that can be assumed to have meaningful centroids (> 5). Notice how this can be quite small even for a batch of 500 samples. We find that a batch of 2000 samples is a decent trade off that achieves good performance.

ℓ_2 normalized embeddings f_i (*i.e.* $\mathcal{F} = \mathbb{S}^{D-1}$) help improve performance and are used in our model. Without the ℓ_2 normalization, our method creates 71 clusters with NMI: 74.57 and WCP: 83.07 ($\sim 2.5\%$ lower).

Single face image at training. We average base CNN representations of face images in a track at test time, while at training, we feed single images. This seems conflicting. However, when we choose to average a random half subset of track images during training, the performance is much worse with 124 clusters and a 7% lower NMI (absolute).

Complexity. During BCL training, each sample is compared only to the centers of clusters/categories. Thus, BCL has complexity linear in the number of samples and number of categories. This is much lower than most baselines that compare samples with samples. We report the wall clock time (average of 3 runs) taken to compute various losses for one epoch – Prototypical: 12.3s; Contrastive: 15.5s; LDML: 15.5s; Triplet: 50.8s; and BCL: 9.9s.

5.3. Evaluation on Test Set

We present statistics of the test set episodes in Table 5, rows 1-6. In particular, note how some episodes have a large

		BBT						BUFFY						BBT	BUFFY	BOTH
		S1E1	S1E2	S1E3	S1E4	S1E5	S1E6	S5E1	S5E2	S5E3	S5E4	S5E5	S5E6	6 ep.	6 ep.	12 ep.
1	#Ch	8	6	26	28	25	37	13	22	15	32	38	45	103	109	212
2	#Named Ch	6	5	7	8	6	6	11	12	13	14	13	17	11	26	37
3	#Unk Ch	2	1	19	20	19	31	2	10	2	18	25	28	92	83	175
4	#T	656	615	660	613	524	840	795	993	1194	898	840	1112	3908	5832	9740
5	#Named T	647	613	562	568	463	651	786	866	1185	852	733	1055	3504	5477	8981
6	#Unk T	9	2	98	45	61	189	9	127	9	46	107	57	404	355	759
CrossEntropy Loss																
7	#Cl	23	24	37	38	26	37	43	39	58	56	49	52	130	194	323
8	NMI	67.42	64.57	64.87	69.73	72.52	63.02	63.14	59.58	59.07	61.44	60.52	61.78	57.91	55.58	60.33
9	WCP	96.80	90.57	86.36	87.93	86.83	73.81	86.67	69.99	78.48	79.73	78.10	70.68	86.59	74.57	76.05
Logistic Discriminant Metric Learning [12]																
10	#Cl	14	15	19	25	20	30	25	31	28	29	31	30	62	82	116
11	NMI	66.42	53.21	66.59	65.33	73.06	55.77	63.57	53.38	58.54	59.52	52.68	56.50	53.15	50.65	51.97
12	WCP	92.23	82.28	74.70	79.61	86.07	62.86	83.02	58.71	71.69	67.59	59.17	59.80	74.33	61.01	58.14
Contrastive Loss [5]																
13	#Cl	14	13	17	22	19	32	22	30	26	29	29	27	60	71	110
14	NMI	62.45	63.69	61.77	65.55	71.38	55.68	61.00	53.94	58.15	53.42	53.59	52.01	58.94	49.15	51.53
15	WCP	90.70	86.99	64.85	76.35	75.57	65.95	77.86	56.09	67.59	60.80	62.02	50.36	77.53	57.30	48.81
Triplet Loss [36]																
16	#Cl	9	12	15	16	13	23	23	24	25	22	23	26	51	73	111
17	NMI	88.13	71.23	79.83	76.71	85.77	69.34	73.60	64.22	66.24	63.61	67.88	65.49	67.94	59.74	64.79
18	WCP	98.48	95.28	90.15	83.69	89.69	76.67	88.68	67.77	81.99	69.71	77.74	68.71	87.31	68.69	71.34
Prototypical Loss [41]																
19	#Cl	12	15	22	28	18	41	32	32	20	35	40	36	87	123	197
20	NMI	82.29	75.12	83.74	80.29	91.36	74.32	74.23	71.02	76.16	70.46	76.63	73.47	70.43	64.99	70.23
21	WCP	96.19	97.56	93.79	91.03	94.66	86.67	90.19	80.16	82.50	81.85	88.69	78.24	90.56	80.52	82.80
Ball Cluster Learning (Ours)																
22	#Cl	7	8	16	18	11	23	17	16	18	22	26	22	47	71	116
23	NMI	95.81	87.25	88.38	76.59	92.21	74.19	81.78	77.60	77.64	78.13	79.72	78.15	73.22	71.23	75.32
24	WCP	98.63	98.54	90.61	86.95	89.12	81.07	92.08	79.76	84.00	84.97	89.05	80.58	89.36	83.62	82.81
Ball Cluster Learning (Ours) + Fine-tune with automatically obtained positive/negative pairs																
25	#Cl	9	8	24	24	21	36	23	27	25	36	38	40	69	78	126
26	NMI	97.34	97.80	94.00	90.42	95.83	83.32	84.59	82.59	78.76	77.58	81.71	79.51	88.26	77.05	80.42
27	WCP	99.24	99.67	96.06	96.08	97.71	90.36	94.97	88.12	90.28	86.19	90.24	88.13	94.11	86.64	85.84

Table 5. Clustering performance on episodes of the test set. S1E2 corresponds to season 1 and episode 2. The last three columns show results on datasets created by combining tracks from several episodes. *Name* refers to primary and secondary named characters; *Unk* refers to background characters; #Ch is number of characters; #T is number of tracks; and #Cl is number of predicted clusters and should be close to the number of characters (row 1). Read this table by looking at each column, and seeing which method is able to predict the number of clusters and has high NMI and WCP scores.

		BBT 6 ep.	BUFFY 6 ep.	ALL 12 ep.
BCL	<i>K</i> -means	60.5 (92.0)	66.7 (87.3)	68.7 (88.0)
BCL	HAC	70.6 (93.0)	69.1 (85.3)	72.5 (86.2)
PRO	<i>K</i> -means	60.7 (91.3)	64.5 (85.4)	66.8 (85.6)
PRO	HAC	68.3 (91.1)	65.8 (80.0)	70.3 (83.3)

Table 6. NMI and WCP performances of our approach (BCL) and prototypical loss (PRO) when the number of clusters is known.

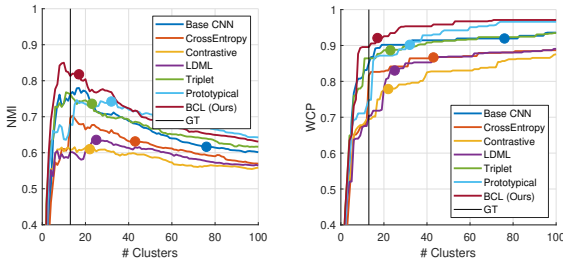


Figure 5. NMI and WCP vs. number of clusters on Buffy S5E1. Circles indicate operating points (*i.e.* number of predicted clusters for the methods), our method uses the HAC threshold $4b$, while all others are using the threshold tuned to give 66 clusters on the validation set. Best seen in color.

number of background characters (*e.g.* 31 for BBT-S1E6) while others do not (*e.g.* 2 for BUFFY-S5E1). The last three columns refer to larger and arguably harder⁴ datasets created by combining tracks of several episodes. In addition to Table 5, we also plot NMI and WCP vs. number of clusters in Fig. 5. Below, we discuss each loss in detail.

CrossEntropy loss (CE). CE can be seen as a (logistic) regression problem that merges all the similar examples to a single one-hot vector. We believe this is a reason why base CNN representations are quite good at clustering (blue curve in Fig. 5) when the number of characters is known. However, using a threshold on validation to choose an operating point results in much lower performance (76 clusters instead of 13). To further test this hypothesis, we train an MLP φ_θ to classify among our training set of actors, and use activations from the last layer as embeddings. The orange curve in Fig. 5 is lower than the base model (blue) indicating that training with more characters may have helped the base model. Nevertheless, choosing an operating point is difficult. Results in Table 5

⁴The combined episode datasets have many more background characters, while tracks from recurring characters collapse onto each other. This further skews cluster membership, with the largest cluster being several thousand tracks, and the smallest still having one track.

rows 7-9 show that the CE over-clusters (create many more clusters than GT). Directly using base CNN representations also results in many clusters (see supplementary).

Verification losses. Next, we analyze LDML, contrastive, and triplet losses (Table 5 rows 10-18). While these losses are often used to perform clustering, they are not designed for it [47]. We see two major features: (i) unlike BCL, estimating the number of clusters is not a built-in feature and requires choosing a threshold on the validation set that may be unreliable; and (ii) early errors in the iterative merging can really harm the overall composition. We observe that triplet loss consistently achieves higher NMI and better estimates for number of clusters than contrastive and LDML.

Prototypical loss (PRO) vs. BCL. Similar to verification losses (above), PRO works best when the number of clusters is known (*e.g.* for few-shot learning). The loss has strong ties with K -means, and optimizes the space to create well separated K clusters [20]. Interestingly, in our experiments, ℓ_2 normalizing embeddings reduced the performance of PRO by over 15% NMI. We report PRO scores for non-normalized representations, that are also more stable when transferring a threshold based on the validation set. In fact, by comparing Table 5 row 19 with row 1, we see that PRO over-estimates the number of clusters when there are few background characters (BCL, row 22, works well here), but performs better in episodes with several background characters.

While PRO estimates more clusters, that does not translate to better assignments. For example, on BUFFY-S5E4, PRO predicts 13 more clusters than BCL (35 vs. 22) and is closer to the ground-truth 32 clusters, but attains 7.7% lower NMI and 3% lower WCP. A lower purity while having more clusters is a strong indicator of bad clustering.

We also compare performance between PRO and BCL when the number of clusters K is known (see Table 6). BCL is able to consistently outperform both K -means or HAC clustering methods for the prototypical loss. We also tried extensions of K -means that automatically determine the number of clusters in an unsupervised way [14, 32] when the representations are fixed. Their performance was worse than our method of choosing a threshold on the validation set. Additional comparisons are in the supplementary material.

Qualitative. Fig. 6 visualizes clusters created by BCL (top) vs. those with PRO (bottom) on BBT-S1E1. BCL predicts 7 clusters in comparison to the ground-truth 8, and merges the singleton track of a background girl (C4 in PRO) with Penny (C3 in BCL). Both methods find the other unnamed character - C4 in BCL, C6 in PRO. While BCL merges few tracks of Sheldon and Kurt (C1), PRO is able to find Kurt (C7). However, PRO splits clusters for Raj (C1, C8), Penny (C3, C11), and Leonard (C2, C10).

Fine-tuning on each episode. Our model can be applied directly to several different datasets by using the learned threshold 4b without fine-tuning, this is a major advantage.

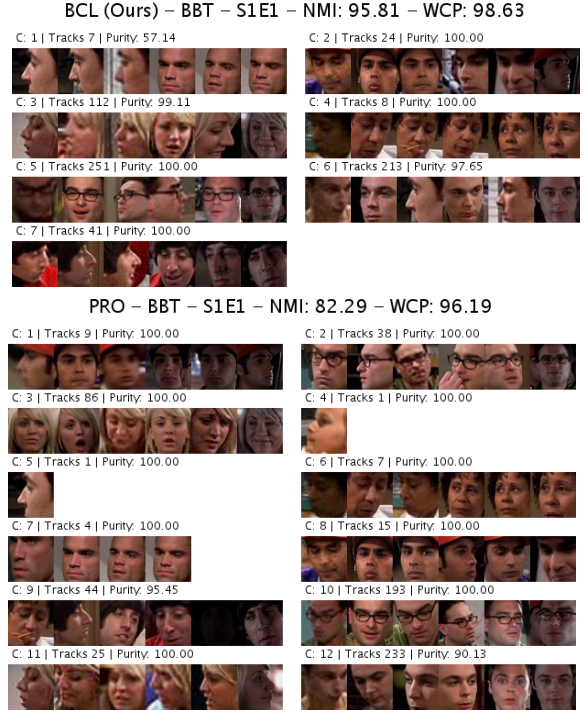


Figure 6. Visualizing clusters created by BCL (top) and PRO (bottom) for BBT-S1E1. Refer to supp. material for other episodes.

Following previous work that uses positive and negative pairs obtained automatically from each episode [6, 43, 54], BCL can be easily modified to fine-tune our model and make it cast-specific. Shots with background characters are often crowded (multiple faces), and negative constraints among them can help resolve confusion. Table 5 rows 25-27 show the overall performance improves after fine-tuning; importantly, the estimated number of characters (row 25) is much closer to the ground-truth (row 1). Details of the fine-tuning procedure and comparison against fine-tuned baselines is in the supplementary material.

6. Conclusion

We presented *Ball Cluster Learning* - a supervised approach to carve the representation space into balls of an equal radius. We showed how the radius is related to the stopping criterion used in agglomerative clustering methods, and evaluated this approach for clustering face tracks in videos. In particular, we considered a realistic setup where the number of clusters is not known, and tracks from all characters (main or otherwise) are included. We reviewed several metric learning approaches and adapted them to this clustering setup. BCL shows promising results, and to the best of our knowledge is the first approach that learns a threshold that can be used directly to estimate the number of clusters.

Acknowledgments. This work was supported by the MSR-Inria joint lab, the Louis-Vuitton - ENS Chair on AI, DARPA Explainable AI (XAI), NSERC, and Samsung.

References

- [1] Rahaf Aljundi, Punarjay Chakravarty, and Tinne Tuytelaars. Who’s that Actor? Automatic Labelling of Actors in TV series starting from IMDB Images. In *Asian Conference on Computer Vision (ACCV)*, 2016. 1, 2
- [2] Daniel Aloise, Amit Deshpande, Pierre Hansen, and Preyas Popat. NP-hardness of Euclidean Sum-of-squares Clustering. *Machine Learning*, 75(2):245–248, 2009. 4
- [3] Martin Bäuml, Makarand Tapaswi, and Rainer Stiefelhof. Semi-supervised Learning with Constraints for Person Identification in Multimedia Data. In *Conference on Computer Vision and Pattern Recognition (CVPR)*, 2013. 1, 2, 5
- [4] Qiong Cao, Li Shen, Weidi Xie, Omkar M. Parkhi, and Andrew Zisserman. VGGFace2: A dataset for recognising faces across pose and age. In *Automatic Face and Gesture Recognition (FG)*, 2018. 1, 5
- [5] Sumit Chopra, Raia Hadsell, and Yann LeCun. Learning a Similarity Metric Discriminatively, with Application to Face Verification. In *Conference on Computer Vision and Pattern Recognition (CVPR)*, 2005. 2, 4, 7, 14
- [6] Ramazan Gokberk Cinbis, Jakob Verbeek, and Cordelia Schmid. Unsupervised Metric Learning for Face Identification in TV Video. In *International Conference on Computer Vision (ICCV)*, 2011. 1, 2, 8, 11
- [7] Timothee Cour, Benjamin Sapp, Akash Nagle, and Ben Taskar. Talking Pictures: Temporal Grouping and Dialog-Supervised Person Recognition. In *Conference on Computer Vision and Pattern Recognition (CVPR)*, 2010. 1, 2
- [8] Daniel Defays. An Efficient Algorithm for a Complete Link Method. *The Computer Journal*, 20(4):364–366, 1977. 4
- [9] Mark Everingham, Josef Sivic, and Andrew Zisserman. “Hello! My name is ... Buffy” – Automatic Naming of Characters in TV Video. In *British Machine Vision Conference (BMVC)*, 2006. 1, 2
- [10] Kamran Ghasedi Dizaji, Amirhossein Herandi, Cheng Deng, Weidong Cai, and Heng Huang. Deep Clustering via Joint Convolutional Autoencoder Embedding and Relative Entropy Minimization. In *International Conference on Computer Vision (ICCV)*, 2017. 2
- [11] Joris Guérin, Olivier Gibaru, Stéphane Thiery, and Eric Nyiri. CNN features are also great at unsupervised classification. *arXiv preprint, arXiv:1707.01700*, 2017. 2
- [12] Matthieu Guillaumin, Jakob Verbeek, and Cordelia Schmid. Is that you? Metric Learning Approaches for Face Identification. In *International Conference on Computer Vision (ICCV)*, 2009. 2, 4, 7
- [13] Yandong Guo, Lei Zhang, Yuxiao Hu, Xiaodong He, and Jianfeng Gao. MS-Celeb-1M: A Dataset and Benchmark for Large Scale Face Recognition. In *European Conference on Computer Vision (ECCV)*, 2016. 5
- [14] Greg Hamerly and Charles Elkan. Learning the k in k-means. In *Advances in Neural Information Processing Systems (NIPS)*, 2004. 8, 11, 12
- [15] Monica-Laura Haurilet, Makarand Tapaswi, Ziad Al-Halah, and Rainer Stiefelhof. Naming TV Characters by Watching and Analyzing Dialogs. In *Winter Conference on Applications of Computer Vision (WACV)*, 2016. 1, 2
- [16] Kaiming He, Xiangyu Zhang, Shaoqing Ren, and Jian Sun. Deep Residual Learning for Image Recognition. In *Conference on Computer Vision and Pattern Recognition (CVPR)*, 2016. 5
- [17] Jie Hu, Li Shen, and Gang Sun. Squeeze-and-Excitation Networks. In *Conference on Computer Vision and Pattern Recognition (CVPR)*, 2018. 5
- [18] SouYoung Jin, Hang Su, Chris Stauffer, and Erik Learned-Miller. End-to-end Face Detection and Cast Grouping in Movies using Erdős–Rényi Clustering. In *International Conference on Computer Vision (ICCV)*, 2017. 1, 2, 5
- [19] Prakhhar Kulshreshtha and Tanaya Guha. An Online Algorithm for Constrained Face Clustering in Videos. In *International Conference in Image Processing (ICIP)*, 2018. 2
- [20] Marc T. Law, Jake Snell, Amir M. Farahmand, Raquel Urtasun, and Richard S Zemel. Dimensionality reduction for representing the knowledge of probabilistic models. In *International Conference on Learning Representations (ICLR)*, 2019. 2, 8
- [21] Marc T. Law, Raquel Urtasun, and Richard S. Zemel. Deep spectral clustering learning. In *International Conference on Machine Learning (ICML)*, volume 70, pages 1985–1994, 2017. 2
- [22] Jie Lei, Licheng Yu, Mohit Bansal, and Tamara L Berg. TVQA: Localized, Compositional Video Question Answering. In *Empirical Methods in Natural Language Processing (EMNLP)*, 2018. 1
- [23] Yu Liu, Junjie Yan, and Wanli Ouyang. Quality Aware Network for Set to Set Recognition. In *Conference on Computer Vision and Pattern Recognition (CVPR)*, 2017. 2, 5
- [24] Stuart Lloyd. Least Squares Quantization in PCM. *IEEE Transactions on Info. Theory*, 28(2):129–137, 1982. 4
- [25] Christopher D. Manning, Prabhakar Raghavan, and Hinrich Schütze. *Introduction to Information Retrieval (chapter 16)*. Cambridge University Press, 2008. 6
- [26] Thomas Mensink, Jakob Verbeek, Florent Perronnin, and Gabriela Csurka. Metric Learning for Large Scale Image Classification: Generalizing to New Classes at Near-zero Cost. In *European Conference on Computer Vision (ECCV)*, 2012. 2
- [27] Erxue Min, Xifeng Guo, Qiang Liu, Gen Zhang, Jianjing Cui, and Jun Long. A survey of clustering with deep learning: From the perspective of network architecture. *IEEE Access*, 6:39501–39514, 2018. 2
- [28] Arsha Nagrani, Samuel Albanie, and Andrew Zisserman. Learnable PINs: Cross-Modal Embeddings for Person Identity. In *European Conference on Computer Vision (ECCV)*, 2018. 2
- [29] Arsha Nagrani and Andrew Zisserman. From Benedict Cumberbatch to Sherlock Holmes: Character Identification in TV series without a Script. In *British Machine Vision Conference (BMVC)*, 2017. 1, 2
- [30] Omkar M. Parkhi, Karen Simonyan, Andrea Vedaldi, and Andrew Zisserman. A Compact and Discriminative Face Track Descriptor. In *Conference on Computer Vision and Pattern Recognition (CVPR)*, 2014. 2, 5

- [31] Omkar M. Parkhi, Andrea Vedaldi, and Andrew Zisserman. Deep Face Recognition. In *British Machine Vision Conference (BMVC)*, 2015. 2
- [32] Dan Pelleg and Andrew Moore. X-means: Extending k-means with efficient estimation of the number of clusters. In *International Conference on Machine Learning (ICML)*, 2000. 8, 11, 12
- [33] Vignesh Ramanathan, Armand Joulin, Percy Liang, and Li Fei-Fei. Linking People in Videos with “Their” Names Using Coreference Resolution. In *European Conference on Computer Vision (ECCV)*, 2014. 2
- [34] Anna Rohrbach, Marcus Rohrbach, Siyu Tang, Seong Joon Oh, and Bernt Schiele. Generating Descriptions with Grounded and Co-Referenced People. In *Conference on Computer Vision and Pattern Recognition (CVPR)*, 2017. 1
- [35] Anna Rohrbach, Atousa Torabi, Marcus Rohrbach, Niket Tandon, Christopher Pal, Hugo Larochelle, Aaron Courville, and Bernt Schiele. Movie Description. *International Journal of Computer Vision (IJCV)*, 123(1):94–120, 2017. 1
- [36] Florian Schroff, Dmitry Kalenichenko, and James Philbin. Facenet: A Unified Embedding for Face Recognition and Clustering. In *Conference on Computer Vision and Pattern Recognition (CVPR)*, 2015. 2, 4, 7, 11, 12, 14
- [37] Matthew Schultz and Thorsten Joachims. Learning a Distance Metric from Relative Comparisons. In *Advances in Neural Information Processing Systems (NIPS)*, 2004. 2
- [38] Vivek Sharma, M. Saquib Sarfraz, and Rainer Stiefelhausen. A Simple and Effective Technique for Face Clustering in TV Series. In *Workshop at Conference on Computer Vision and Pattern Recognition (CVPRW)*, 2017. 1
- [39] Vivek Sharma, Makarand Tapaswi, M. Saquib Sarfraz, and Rainer Stiefelhausen. Self-Supervised Learning of Face Representations for Video Face Clustering. In *Automatic Face and Gesture Recognition (FG)*, 2019. 2, 5
- [40] Josef Sivic, Mark Everingham, and Andrew Zisserman. “Who are you?” – Learning person specific classifiers from video. In *Conference on Computer Vision and Pattern Recognition (CVPR)*, 2009. 2
- [41] Jake Snell, Kevin Swersky, and Richard Zemel. Prototypical Networks for Few-shot Learning. In *Advances in Neural Information Processing Systems (NIPS)*, 2017. 2, 4, 7, 11, 12, 14
- [42] Makarand Tapaswi, Martin Bäumel, and Rainer Stiefelhausen. “Knock! Knock! Who is it?” Probabilistic Person Identification in TV series. In *Conference on Computer Vision and Pattern Recognition (CVPR)*, 2012. 2
- [43] Makarand Tapaswi, Omkar M. Parkhi, Esa Rahtu, Eric Sommerlade, Rainer Stiefelhausen, and Andrew Zisserman. Total Cluster: A person agnostic clustering method for broadcast videos. In *Indian Conference on Computer Vision, Graphics and Image Processing (ICVGIP)*, 2014. 2, 6, 8, 11
- [44] Makarand Tapaswi, Yukun Zhu, Rainer Stiefelhausen, Antonio Torralba, Raquel Urtasun, and Sanja Fidler. MovieQA: Understanding Stories in Movies through Question-Answering. In *Conference on Computer Vision and Pattern Recognition (CVPR)*, 2016. 1
- [45] Paul Vicol, Makarand Tapaswi, Lluís Castrejón, and Sanja Fidler. MovieGraphs: Towards Understanding Human-Centric Situations from Videos. In *Conference on Computer Vision and Pattern Recognition (CVPR)*, 2018. 1, 2, 5
- [46] Feng Wang, Xiang Xiang, Jian Cheng, and Alan Loddon Yuille. NormFace: 12 Hypersphere Embedding for Face Verification. In *ACM International Conference on Multimedia (ACM MM)*, 2017. 2, 3, 4
- [47] Jixuan Wang, Kuan-Chieh Wang, Marc T. Law, Frank Rudzicz, and Michael Brudno. Centroid-based deep metric learning for speaker recognition. In *International Conference on Acoustics, Speech and Signal Processing (ICASSP)*, 2019. 8
- [48] Ruiping Wang, Huimin Guo, Larry S. Davis, and Qionghai Dai. Covariance Discriminative Learning: A Natural and Efficient Approach to Image Set Classification. In *Conference on Computer Vision and Pattern Recognition (CVPR)*, 2012. 2, 5
- [49] Baoyuan Wu, Siwei Lyu, Bao-Gang Hu, and Qiang Ji. Simultaneous Clustering and Tracklet Linking for Multi-face Tracking in Videos. In *International Conference on Computer Vision (ICCV)*, 2013. 2, 11
- [50] Baoyuan Wu, Yifan Zhang, Bao-Gang Hu, and Qiang Ji. Constrained Clustering and its Application to Face Clustering in Videos. In *Conference on Computer Vision and Pattern Recognition (CVPR)*, 2013. 2, 11
- [51] Shijie Xiao, Minghui Tan, and Dong Xu. Weighted Block-sparse Low Rank Representation for Face Clustering in Videos. In *European Conference on Computer Vision (ECCV)*, 2014. 2, 11
- [52] Jianwei Yang, Devi Parikh, and Dhruv Batra. Joint unsupervised learning of deep representations and image clusters. In *Conference on Computer Vision and Pattern Recognition (CVPR)*, 2016. 2
- [53] Jiaolong Yang, Peiran Ren, Dongqing Zhang, Dong Chen, Fang Wen, Hongdong Li, and Gang Hua. Neural Aggregation Network for Video Face Recognition. In *Conference on Computer Vision and Pattern Recognition (CVPR)*, 2017. 2, 5
- [54] Shun Zhang, Yihong Gong, and Jinjun Wang. Deep Metric Learning with Improved Triplet Loss for Face Clustering in Videos. In *Pacific Rim Conference on Multimedia*, 2016. 2, 8, 11
- [55] Zhanpeng Zhang, Ping Luo, Chen Change Loy, and Xiaoou Tang. Joint Face Representation Adaptation and Clustering in Videos. In *European Conference on Computer Vision (ECCV)*, 2016. 1, 2, 5, 6, 11

Supplementary Material

In this document, we discuss how we fine-tune our models on the test episodes using the BCL loss. We also briefly discuss the challenges to fine-tune using triplet or prototypical losses, but show that they can use the constraints inspired by BCL in Sec. A. Additionally, we will show that variants of K-means that aim to predict the number of clusters such as X-means [32] and G-means [14] perform worse than our proposed method (Sec. B). Finally, we present additional quantitative and qualitative results on the TV series episodes introduced in the main paper in Sec. C.

A. Fine-tuning on test episodes

As discussed in the related work section, many clustering approaches use unsupervised constraints that arise from the video to learn cast-specific metrics [6, 43, 49, 50, 51, 54, 55]. The positive constraints are obtained from face images within a track that are considered similar; and negative constraints from faces that appear at the same time in the video that can be assumed to be dissimilar. Note that most previous works know the number of clusters, and use the constraints to improve the distance metric.

In the following, we show how our method can be modified to work with such positive and negative constraints. We also discuss the limitations of the baselines for fine-tuning, but propose an alternative that uses BCL pair-wise constraints.

Ball Cluster Learning. Recall that our constraints are originally based on cluster samples and their centroids. For all $x_i \in \mathcal{C}_k$, BCL aims to satisfy $d^2(\mathbf{f}_i, \mu_k) < b$ and $d^2(\mathbf{f}_i, \mu_v) > \gamma$, where $\gamma = 9b + \epsilon$ and $x_i \notin \mathcal{C}_v$.

For a positive pair $x_i \in \mathcal{C}_k, x_j \in \mathcal{C}_k$, and a negative counterpart $x_u \in \mathcal{C}_v$, the centroid constraints can be modified as:

$$d^2(\mathbf{f}_i, \mathbf{f}_j) < 4b \text{ and } d^2(\mathbf{f}_i, \mathbf{f}_u) > 4b + \epsilon. \quad (11)$$

In practice, as the model is already trained, we wish to only fine-tune on the positive and negative pairs. In most cases, the positive constraints are already satisfied, and using the relaxed constraint hurt performance. Thus, we use: $d^2(\mathbf{f}_i, \mathbf{f}_j) < \min(d_{\text{ori}}^2(\mathbf{f}_i, \mathbf{f}_j), 4b)$, where $d_{\text{ori}}^2(\mathbf{f}_i, \mathbf{f}_j)$ is the distance between the pair prior to fine-tuning. The constraints are formulated as loss functions to train the model by using the $[\cdot]_+ = \max(0, \cdot)$ operator as before.

We tried an analogous strategy for dissimilar pairs (using $\max(d_{\text{ori}}^2(\mathbf{f}_i, \mathbf{f}_u), 4b + \epsilon)$) but it did not provide significant performance improvement. Thus, we ignored it.

During training, we freeze the ball squared-radius b , use a learning rate of 0.0003 (0.1 times the original), and select a random face image from each track in the pairs (about

1,000 pairs for each episode). The model parameters are updated for a fixed number of iterations (2,000 for all single episodes). As before, we perform clustering by using Hierarchical Agglomerative Clustering (HAC) with complete linkage and distance threshold $\tau = 4b$.

Triplet loss [36] is well suited to train a model with above-mentioned automatically obtained positive and negative pairs. However, it does not involve learning a threshold that can be used directly with HAC (or any clustering). As we are fine-tuning on test episodes, we do not have access to a validation set that would allow us to obtain such a threshold. Furthermore, optimizing performance on each test episode by choosing a new *best* threshold is inappropriate.

To circumvent this, we use the original threshold learned on the validation set τ and formulate pair-wise constraints in a similar manner to BCL. In particular, the positive pairs follow $d^2(\mathbf{f}_i, \mathbf{f}_j) < \tau$ and negative pairs $d^2(\mathbf{f}_i, \mathbf{f}_u) > \tau$. Thus, we fine-tune the model checkpoint trained using the triplet loss with the BCL loss. All other implementation details (learning rate, number of iterations, *etc.*) are same as those used for BCL.

Prototypical loss [41]. Unlike the triplet loss that is designed to work with samples (triplets), the prototypical loss needs class/cluster centroids. It also faces the same challenge of not knowing the number of clusters, or not having a clear stopping criterion for HAC. Nevertheless, as discussed for triplet loss above, we adopt BCL pair-wise constraints for the prototypical loss with the threshold τ chosen on validation. All other details are kept same.

Evaluation. Table 7 presents results of fine-tuning on each episode. For each episode, we see that BCL fine-tuned model (BCL-FT) is able to predict the number of clusters quite accurately. We believe this can be attributed to background characters often appearing simultaneously, providing sufficient negative constraints. On the combined episodes datasets (last three columns of Table 7), the negative constraints are within each episode, and it is not possible to distinguish between background characters across episodes. This explains why BCL predicts fewer clusters than ground-truth.

Both baselines (TRI-FT and PRO-FT) also show good performance improvements after fine-tuning with BCL. With respect to predicting the number of clusters, PRO-FT and BCL-FT seem to have flipped roles, with PRO-FT now predicting fewer clusters after fine-tuning, but over-clustering before fine-tuning (see Table 5 of the main paper). However, note that BCL-FT with more clusters has higher purity, while PRO (no fine-tune) had lower purity even with more clusters (in Table 5).

		BBT						BUFFY						BBT	BUFFY	BOTH
		S1E1	S1E2	S1E3	S1E4	S1E5	S1E6	S5E1	S5E2	S5E3	S5E4	S5E5	S5E6	6 ep.	6 ep.	12 ep.
1	#Ch	8	6	26	28	25	37	13	22	15	32	38	45	103	109	212
Pre-trained Triplet Loss [36] + BCL Fine-tune																
2	#Cl	6	7	13	12	12	23	16	21	16	18	22	23	33	54	73
3	NMI	97.98	97.13	91.22	86.37	95.25	83.38	85.91	82.62	78.98	75.34	76.04	78.66	89.09	76.28	78.95
4	WCP	99.09	99.84	92.73	89.23	94.08	86.31	91.95	87.71	85.76	78.95	80.83	79.59	92.40	81.45	82.26
Pre-trained Prototypical Loss [41] + BCL Fine-tune																
5	#Cl	6	6	19	16	15	41	17	22	21	27	21	34	61	72	113
6	NMI	96.76	97.09	91.43	90.83	95.84	85.38	77.98	83.01	79.29	77.24	81.74	82.31	87.74	79.90	82.81
7	WCP	98.17	99.67	95.00	93.31	94.85	93.69	90.82	87.11	88.86	82.52	84.76	84.80	93.96	85.17	85.26
Pre-trained Ball Cluster Learning (Ours) + BCL Fine-tune																
8	#Cl	9	8	24	24	21	36	23	27	25	36	38	40	69	78	126
9	NMI	97.34	97.80	94.00	90.42	95.83	83.32	84.59	82.59	78.76	77.58	81.71	79.51	88.26	77.05	80.42
10	WCP	99.24	99.67	96.06	96.08	97.71	90.36	94.97	88.12	90.28	86.19	90.24	88.13	94.11	86.64	85.84

Table 7. Clustering performance on episodes of the test set, with fine-tuning on the test set. The last three columns show results on datasets created by combining tracks from several episodes. #Ch is the ground-truth number of characters (row 1); and #Cl is number of predicted clusters and should be close to the number of characters. Read this table by looking at each column, and seeing which method is able to predict the number of clusters and has high NMI and WCP scores.

Conclusion. This experiment emphasizes that BCL combines the best of all worlds. Models can be trained with both samples and centroids, or pairs and triplets. Most importantly, BCL learns a threshold to predict the number of clusters automatically. In addition, BCL pair-wise loss can be used to fine-tune models trained with other losses to achieve performance gains.

B. K-means variants

Owing to the popularity of the K -means approach for clustering, there is some work on automatically estimating the number of clusters while performing clustering based on some criterion. In this section, we will look at two such methods and analyze how they work when applied to our challenging datasets. Note that both these methods do not further learn an embedding, but rely on existing features. Thus, we evaluate performance on the Base CNN representations – that are actually quite good (see Table 9), as well as the features learned using our BCL loss function.

X-means [32] In this variant, clustering starts with all samples in the same cluster and splits until some stopping criterion. In particular, at each iteration, a cluster is split into two components. The Bayesian Information Criterion (BIC) is used to decide whether the newly created two clusters are preferred over the original single cluster. Clustering stops when a maximum number of clusters K_{\max} has been crossed, or when further splitting any cluster would result in lowered BIC scores.

Table 8 rows 2-4 show the performance of X-means when using base CNN features, and rows 5-7 when using features trained with BCL loss. We choose K_{\max} to be 40 for the BBT episodes, 80 for BUFFY, 150 for BBT (6 episodes combined) and BUFFY (6 episodes combined), and 300 for

BOTH (all 12 episodes). These are strong upper bounds for all datasets. However, as seen from the results, the method stops the iterations only after crossing the maximum number of clusters in all datasets (*i.e.* all predicted number of clusters are higher than K_{\max}). This, together with the poor NMI scores, suggests that the using BIC may not be a sufficiently strong criterion for a complex dataset.

G-means [14] Similar to X-means, this approach also starts with all samples in one cluster, and iteratively splits them based on some criterion. Different to X-means, the stopping criterion used here determines the “Gaussian-ness” of samples around the cluster centroid. In particular, clusters that have a strong Gaussian shape are not split further, while others (*e.g.* those that may be bimodal) are split into two. This process repeats until no more clusters can be split. The Anderson-Darling test is used to determine whether a distribution is Gaussian.

We present the results of G-means in the second half of Table 8. We see that G-means also fails at reliably estimating the number of clusters, and prefers to overcluster all datasets.

C. Additional evaluation

Base CNN representations. In Table 9, we present the performance of base CNN representations with standard HAC clustering and using a threshold learned on the validation set. These results should be analyzed together with Table 5 of the main paper, but were omitted due to space constraints. Note that the threshold is chosen such that correct number of clusters are created on the validation set. While the base representation is quite good (as seen in NMI and WCP curves), choosing a threshold is an unreliable method and results in over-clustering on the test episodes.

		BBT						BUFFY						BBT	BUFFY	BOTH
		S1E1	S1E2	S1E3	S1E4	S1E5	S1E6	S5E1	S5E2	S5E3	S5E4	S5E5	S5E6	6 ep.	6 ep.	12 ep.
1	#Ch	8	6	26	28	25	37	13	22	15	32	38	45	103	109	212
X-Means on Base CNN representation																
2	#Cl	41	42	45	41	51	48	93	89	90	82	101	91	175	180	327
3	NMI	55.74	56.83	65.75	64.89	66.47	66.51	59.61	66.86	57.56	62.99	61.03	66.23	56.26	62.67	65.85
4	WCP	98.63	97.89	92.73	90.70	94.27	84.64	94.59	90.74	88.86	87.75	88.21	86.15	92.71	87.21	88.68
X-Means on features learned with BCL																
5	#Cl	42	25	45	34	43	44	97	41	81	84	80	91	162	163	313
6	NMI	56.90	62.46	69.82	68.35	71.46	70.08	60.12	72.16	59.99	65.90	66.59	69.72	58.62	63.91	66.63
7	WCP	99.24	97.89	95.45	91.35	96.18	87.38	95.85	88.62	91.04	91.31	92.02	89.48	93.22	88.73	88.87
G-Means on Base CNN representation																
8	#Cl	57	31	56	33	46	67	87	101	117	74	73	101	243	404	567
9	NMI	55.29	62.61	70.41	71.48	71.74	67.00	58.07	66.63	58.34	67.06	63.50	69.08	57.64	61.57	66.07
10	WCP	98.32	96.42	94.85	91.35	94.85	86.55	89.18	89.93	88.94	89.31	87.14	87.68	92.14	87.21	87.95
G-Means on features learned with BCL																
11	#Cl	23	39	41	35	45	79	42	54	75	63	72	106	137	337	481
12	NMI	68.51	64.54	72.74	70.38	73.22	66.18	67.87	61.43	62.88	65.70	66.91	69.09	60.86	61.63	64.42
13	WCP	98.93	98.05	92.42	91.35	94.85	87.02	91.07	71.30	84.00	86.41	88.45	87.86	89.94	85.51	84.06

Table 8. Clustering performance on episodes of the test set using two variants of K-means that predict the number of clusters.

		BBT						BUFFY						BBT	BUFFY	BOTH
		S1E1	S1E2	S1E3	S1E4	S1E5	S1E6	S5E1	S5E2	S5E3	S5E4	S5E5	S5E6	6 ep.	6 ep.	12 ep.
1	#Ch	8	6	26	28	25	37	13	22	15	32	38	45	103	109	212
Base CNN representation																
2	#Cl	36	38	49	51	36	59	76	75	94	93	95	92	200	407	609
3	NMI	59.84	60.60	68.18	69.18	74.85	68.42	61.66	67.94	57.88	65.01	65.59	66.90	59.33	60.00	64.80
4	WCP	97.41	97.72	92.88	92.66	95.42	86.31	91.95	88.02	88.27	89.64	91.31	85.52	93.19	88.08	89.14

Table 9. Clustering performance on episodes of the test set when using base CNN representation.

When K is known. We also present results when (for some reason) the number of clusters K is known. We compare against best performing baselines: triplet and prototypical loss, on all episodes of the test set. Table 10 shows that our method is able to achieve higher NMI and WCP in most cases (12 out of 15). Note that this experiment is presented for completeness, as the main point of BCL is to automatically predict the number of clusters, when K is unknown. All results are without fine-tuning.

Choosing a threshold on train set. As the training set is much larger than validation, it might seem that the baselines may perform better when choosing a threshold on the validation set. However, this is not the case as observed from Table 11. As the MLP φ_θ fits well to the training set a smaller cutoff threshold (distance) is selected resulting in more clusters on unseen data. Thus, it is important to have a separate validation set.

NMI and WCP vs. number of clusters. We plot the NMI and WCP curves for all methods (as in Fig. 5 of the main paper) for each episode of BBT in Fig. 7 and BUFFY in Fig. 8. All results are before fine-tuning. We wish to draw the reader to the following observations:

1. The threshold for prototypical loss is quite stable and

is able to predict the number of clusters well (as was discussed in Table 5 of the main paper). However, the **purity is almost always lower than our method**, indicating that even though it makes more clusters, the formed clusters tend to be more heterogeneous (*i.e.* contain more samples from different categories).

2. Our method shows higher NMI and WCP irrespective of the operating point in most episodes.

3. The base representations have very good performance curves. However, their operating points (chosen based on the validation threshold) are far from the optimal number of clusters. Cross-entropy loss, especially when used with thousands of classes, seems to be effective at learning classification as well as clustering.

Qualitative visualization of clusters. Finally, we visualize the clusters created by Triplet loss (TRI), Prototypical Loss (PRO), and our method Ball Cluster Learning (BCL) on one episode of BBT (Fig. 9) and BUFFY (Fig. 10). Each cluster is visualized by selecting 6 random face tracks (when available), and one face image per track. All results are without fine-tuning.

These figures also throw light on the difficulty of our dataset that includes wide variations in illumination and

Method	Metric	BBT						BUFFY						BBT	BUFFY	ALL
		S1E1	S1E2	S1E3	S1E4	S1E5	S1E6	S5E1	S5E2	S5E3	S5E4	S5E5	S5E6	6 ep.	6 ep.	12 ep.
Triplet Loss [36]																
KM	NMI	73.2	83.4	74.7	70.5	75.5	67.8	74.3	64.7	68.7	64.6	68.8	66.0	57.8	59.2	62.6
KM	WCP	93.6	96.7	93.2	91.4	93.7	83.7	88.1	72.3	80.8	80.1	86.1	78.0	89.7	77.7	80.5
HAC	NMI	88.3	69.0	79.1	76.6	81.9	70.8	76.2	64.1	66.9	64.9	70.7	67.6	64.0	60.1	65.3
HAC	WCP	98.5	79.2	93.0	91.5	94.7	80.4	86.4	67.4	77.3	73.3	84.0	76.5	90.2	72.7	76.9
Prototypical Loss [41]																
KM	NMI	80.8	82.5	76.0	72.3	76.0	69.4	79.5	74.6	74.3	71.9	71.4	72.5	60.7	64.5	66.8
KM	WCP	95.0	95.6	93.6	91.7	94.3	83.7	89.4	84.2	83.7	86.0	88.9	84.7	91.3	85.4	85.6
HAC	NMI	87.6	86.6	83.1	80.3	89.2	74.0	67.9	68.4	77.4	70.6	76.5	73.8	68.3	65.8	70.3
HAC	WCP	94.7	94.8	94.2	91.0	96.2	85.2	74.8	73.0	79.9	81.2	85.1	82.8	91.1	80.0	83.3
Ball Cluster Learning (Ours)																
KM	NMI	83.9	90.1	73.2	70.2	76.9	71.6	78.9	79.1	72.0	72.9	71.6	74.8	60.5	66.7	68.7
KM	WCP	98.5	99.2	92.9	91.2	93.5	86.1	91.6	87.4	81.6	87.6	88.8	87.7	92.0	87.3	88.0
HAC	NMI	92.8	91.9	84.3	78.5	86.1	76.1	81.3	75.3	77.9	75.9	76.9	78.6	70.6	69.1	72.5
HAC	WCP	98.6	98.2	92.6	91.7	96.0	86.7	89.6	81.4	81.4	87.3	91.2	88.5	93.0	85.3	86.2

Table 10. Comparison between models trained with triplet, prototypical, and our approach when the number of clusters is known. We evaluate both K -means (KM) as well as Hierarchical Agglomerative Clustering (HAC) to obtain the appropriate number of clusters. A short version of this appeared as Table 6 in the main paper.

Thresh Set	BBT						BUFFY					
	S1E1	S1E2	S1E3	S1E4	S1E5	S1E6	S5E1	S5E2	S5E3	S5E4	S5E5	S5E6
#Ch	8	6	26	28	25	37	13	22	15	32	38	45
Contrastive Loss [5]												
train	374 (40.6)	382 (41.0)	411 (52.5)	443 (51.7)	341 (54.3)	629 (56.7)	605 (48.1)	721 (55.0)	862 (46.8)	694 (53.5)	608 (53.7)	725 (57.9)
val	14 (62.5)	13 (63.7)	17 (61.8)	22 (65.6)	19 (71.4)	32 (55.7)	22 (61.0)	30 (53.9)	26 (58.2)	29 (53.4)	29 (53.6)	27 (52.0)
Triplet Loss [36]												
train	28 (65.5)	31 (63.4)	38 (74.6)	44 (74.1)	39 (78.2)	72 (68.3)	64 (65.0)	73 (64.9)	77 (60.1)	67 (63.6)	66 (69.4)	79 (68.4)
val	9 (88.1)	12 (71.2)	15 (79.8)	16 (76.7)	13 (85.8)	23 (69.3)	23 (73.6)	24 (64.2)	25 (66.2)	22 (63.6)	23 (67.9)	26 (65.5)
Prototypical Loss [41]												
train	19 (74.6)	25 (69.3)	35 (77.4)	39 (76.6)	27 (86.6)	63 (73.9)	50 (70.7)	55 (69.7)	43 (67.8)	60 (69.7)	63 (72.7)	65 (74.3)
val	12 (82.3)	15 (75.1)	22 (83.7)	28 (80.3)	18 (91.4)	41 (74.3)	32 (74.2)	32 (71.0)	20 (76.2)	35 (70.5)	40 (76.6)	36 (73.5)

Table 11. Choosing the HAC threshold on train vs. validation set. Showing the number of predicted clusters and NMI. Ideal number of clusters is presented in the first row. Note how it is beneficial to have a separate validation set, as overfitting on training can lead to selection of smaller thresholds.

pose. Tracks, their labels and features, and our implementation of BCL is available at https://github.com/makarandtapaswi/BallClustering_ICCV2019.

In Fig. 9, BCL achieves close to the correct number of clusters, and separates the unknown character with just 2 tracks (C:2). Both triplet and prototypical losses lead to over clustering. *E.g.* Leonard is split to C:1, C:6, C:7 and C:12 in triplet loss, and C:1, C:4, C:6, C:11, C:13 when using

prototypical loss.

BUFFY-S5E3 (Fig. 10) is a unique episode in which one of the lead characters *Xander* is duplicated due to a magic spell (the duplicate is played by the actor’s identical twin). Nevertheless, we see that BCL achieves reasonable performance, and is able to find minor characters (Joyce C:9, the building manager C:10), as well as isolate one of the background characters (C:11).

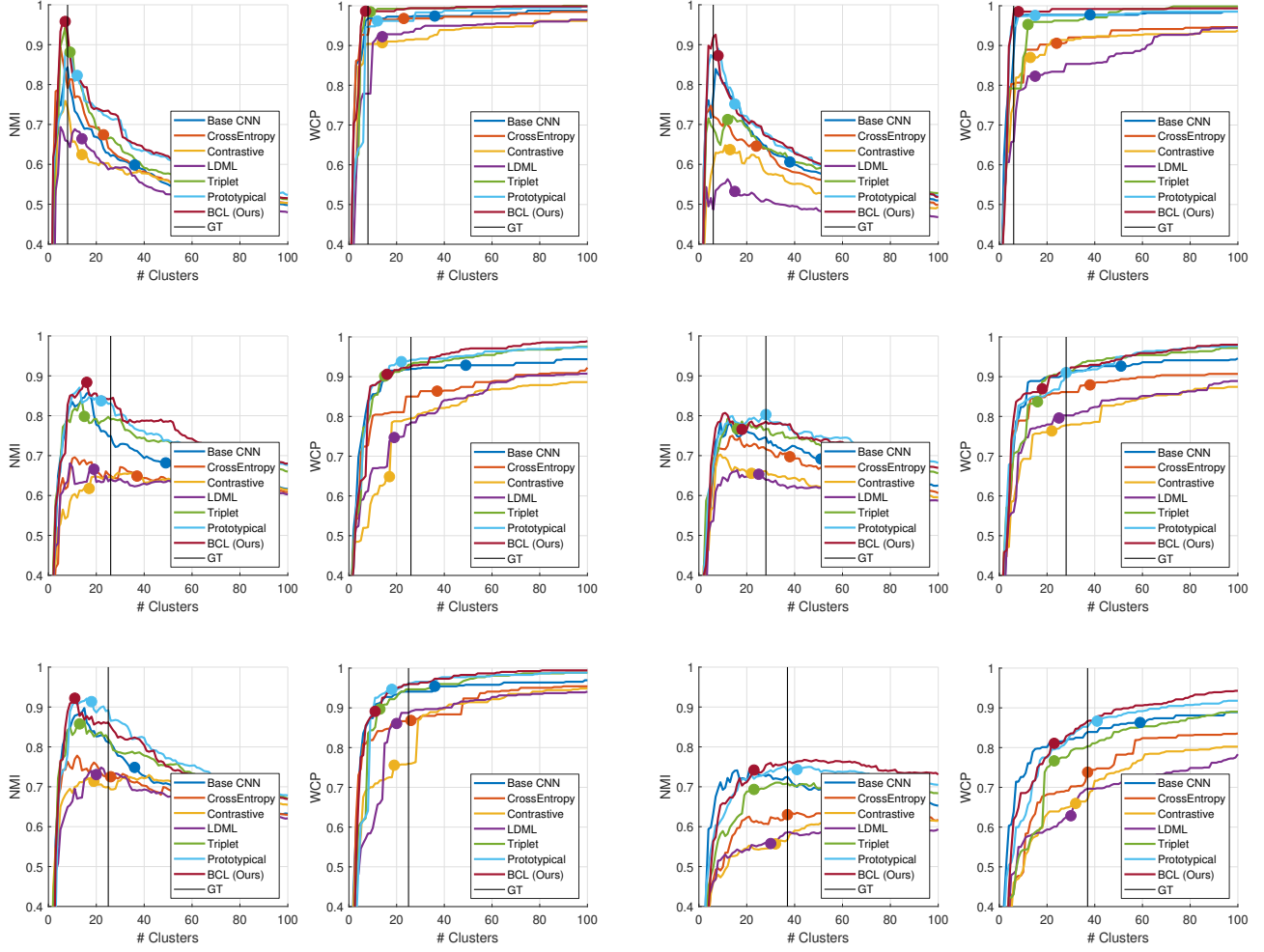


Figure 7. NMI and WCP vs. number of clusters for BBT-S1E1 to S1E6 (left to right, top to bottom). Circles indicate operating points (*i.e.* number of predicted clusters for the methods), our method uses the HAC threshold $4b$, while all others are using the threshold tuned to give 66 clusters on the validation set. Best seen in color.

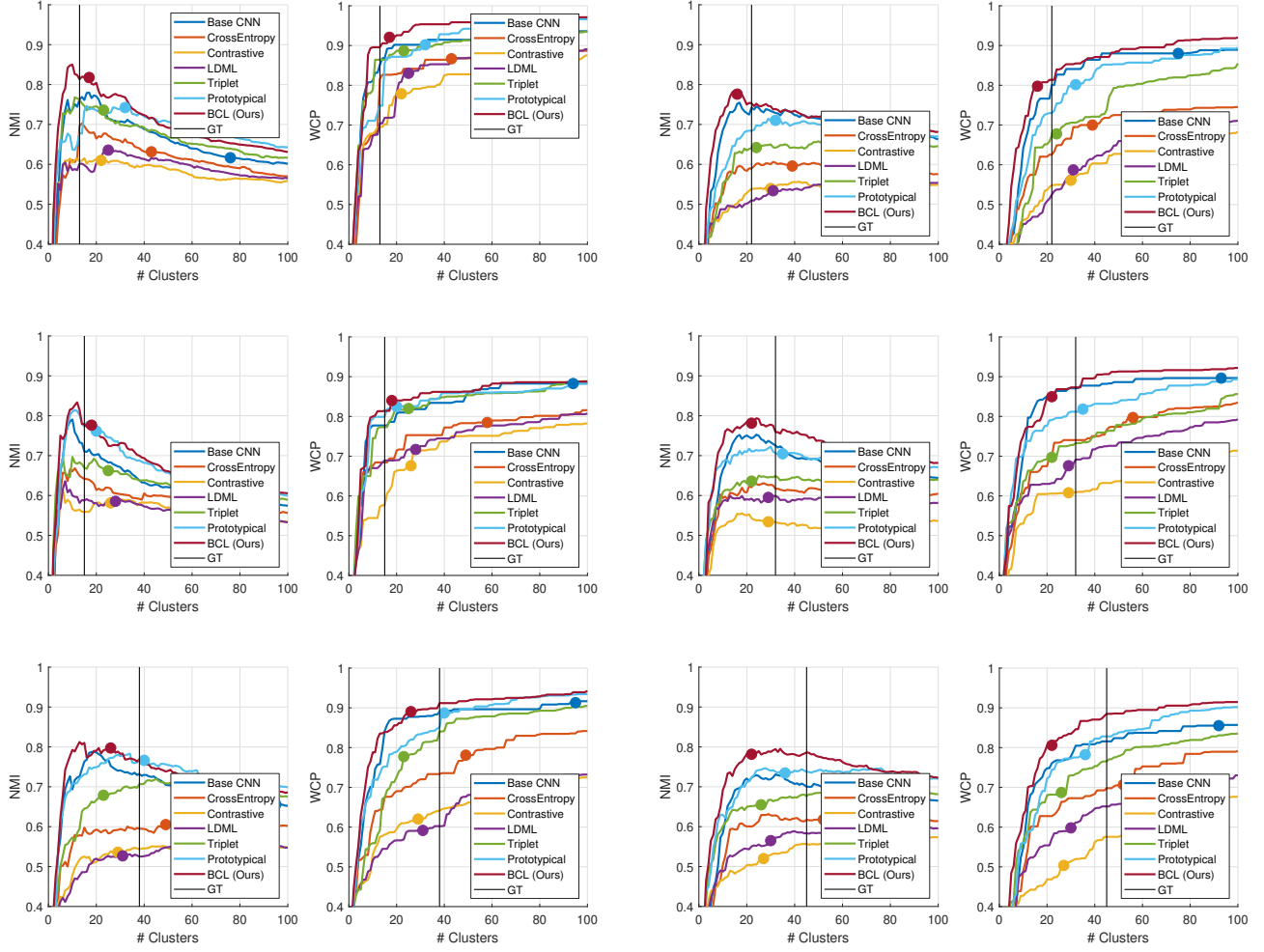
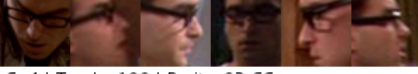


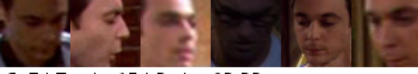
Figure 8. NMI and WCP vs. number of clusters for BUFFY-S5E1 to S5E6 (left to right, top to bottom). Circles indicate operating points (*i.e.* number of predicted clusters for the methods), our method uses the HAC threshold $4b$, while all others are using the threshold tuned to give 66 clusters on the validation set. Best seen in color.

TRI – BBT – S1E2 – NMI: 71.23 – WCP: 95.28

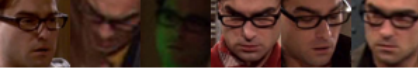
C: 1 | Tracks 72 | Purity: 81.94



C: 4 | Tracks 109 | Purity: 92.66



C: 7 | Tracks 15 | Purity: 93.33



C: 10 | Tracks 54 | Purity: 94.44



C: 2 | Tracks 24 | Purity: 100.00



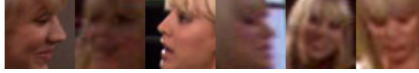
C: 5 | Tracks 60 | Purity: 100.00



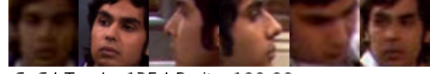
C: 8 | Tracks 44 | Purity: 95.45



C: 11 | Tracks 35 | Purity: 100.00



C: 3 | Tracks 56 | Purity: 100.00



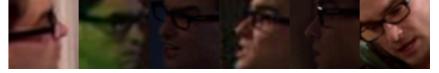
C: 6 | Tracks 125 | Purity: 100.00



C: 9 | Tracks 12 | Purity: 83.33



C: 12 | Tracks 9 | Purity: 100.00



PRO – BBT – S1E2 – NMI: 75.12 – WCP: 97.56

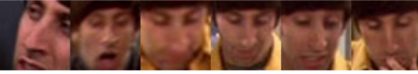
C: 1 | Tracks 57 | Purity: 100.00



C: 4 | Tracks 32 | Purity: 100.00



C: 7 | Tracks 15 | Purity: 100.00



C: 10 | Tracks 5 | Purity: 100.00



C: 13 | Tracks 17 | Purity: 88.24



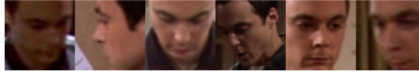
C: 2 | Tracks 11 | Purity: 100.00



C: 5 | Tracks 22 | Purity: 100.00



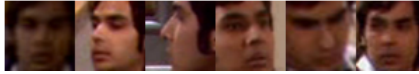
C: 8 | Tracks 178 | Purity: 97.75



C: 11 | Tracks 72 | Purity: 98.61



C: 14 | Tracks 43 | Purity: 93.02



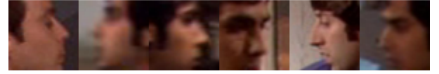
C: 3 | Tracks 1 | Purity: 100.00



C: 6 | Tracks 36 | Purity: 100.00



C: 9 | Tracks 9 | Purity: 44.44



C: 12 | Tracks 84 | Purity: 100.00



C: 15 | Tracks 33 | Purity: 100.00



BCL (Ours) – BBT – S1E2 – NMI: 87.25 – WCP: 98.54

C: 1 | Tracks 105 | Purity: 100.00



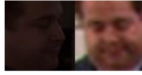
C: 4 | Tracks 36 | Purity: 100.00



C: 7 | Tracks 79 | Purity: 92.41



C: 2 | Tracks 2 | Purity: 100.00



C: 5 | Tracks 213 | Purity: 99.06



C: 8 | Tracks 52 | Purity: 100.00



C: 3 | Tracks 34 | Purity: 97.06



C: 6 | Tracks 94 | Purity: 100.00

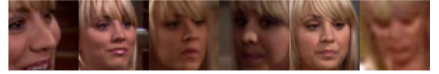


Figure 9. Clusters created by triplet loss (TRI, top), prototypical loss (PRO, middle), and BCL (bottom) on BBT-S1E2. The correct number of clusters is 6.

TRI – BUFFY – S5E3 – NMI: 66.24 – WCP: 81.99



PRO – BUFFY – S5E3 – NMI: 76.16 – WCP: 82.50



BCL (Ours) – BUFFY – S5E3 – NMI: 77.64 – WCP: 84.00



Figure 10. Clusters created by triplet loss (TRI, top), prototypical loss (PRO, middle), and BCL (bottom) on BUFFY-S5E3. The correct number of clusters is 15.